remote sensing

MDPI

Article

Sparse Reconstruction-Based Joint Signal Processing for MIMO-OFDM-IM Integrated Radar and Communication Systems

Yang Wang [1], Yunhe Cao [1,*], Tat-Soon Yeo [2], Yuanhao Cheng [1] and Yulin Zhang [1]

[1] National Key Laboratory of Radar Signal Processing, Xidian University, Xi'an 710071, China; yw_ivy@stu.xidian.edu.cn (Y.W.); chengyh@stu.xidian.edu.cn (Y.C.); zhangyulin@stu.xidian.edu.cn (Y.Z.)
[2] Department of Electrical and Computer Engineering, National University of Singapore, Singapore 119077, Singapore; eleyeots@nus.edu.sg
* Correspondence: caoyunhe@mail.xidian.edu.cn

Abstract: Multiple-input multiple-output orthogonal frequency division multiplexing (MIMO-OFDM) technology is widely used in integrated radar and communication systems (IRCSs). Moreover, index modulation (IM) is a reliable OFDM transmission scheme in the field of communication, which transmits information by arranging several distinguishable constellations. In this paper, we propose a sparse reconstruction-based joint signal processing scheme for integrated MIMO-OFDM-IM systems. Combining the advantages of MIMO and OFDM-IM technologies, the integrated MIMO-OFDM-IM signal design is realized through the reasonable allocation of bits and subcarriers, resulting in better intercarrier interference (ICI) resistance and a higher transmission efficiency. Taking advantage of the sparseness of OFDM-IM, an improved target parameter estimation method based on sparse signal reconstruction is explored to eliminate the influence of empty subcarriers on the matched filtering at the receiver side. In addition, an improved sequential Monte Carlo signal detection method is introduced to realize the efficient detection of communication signals. The simulation results show that the proposed integrated system is 5 dB lower in the peak sidelobe ratio (PSLR) and 1.5×10^5 lower in the number of complex multiplications than the latest MIMO-OFDM system and can achieve almost the same parameter estimation performance. With the same spectral efficiency, it has a lower bit error rate (BER) than existing methods.

Keywords: integrated radar and communications; MIMO-OFDM; index modulation (IM); signal sparsity model; low-complexity detection

check for updates

Citation: Wang, Y.; Cao, Y.; Yeo, T.-S.; Cheng, Y.; Zhang, Y. Sparse Reconstruction-Based Joint Signal Processing for MIMO-OFDM-IM Integrated Radar and Communication Systems. *Remote Sens.* **2024**, *16*, 1773. https://doi.org/10.3390/rs16101773

Academic Editor: Dusan Gleich

Received: 29 March 2024
Revised: 4 May 2024
Accepted: 13 May 2024
Published: 16 May 2024

Copyright: © 2024 by the authors. Licensee MDPI, Basel, Switzerland. This article is an open access article distributed under the terms and conditions of the Creative Commons Attribution (CC BY) license (https://creativecommons.org/licenses/by/4.0/).

1. Introduction

Integrated radar and communication technology has recently seen rapid development and applications in both military and civilian arenas. This technology uses a single transmitted signal to simultaneously perform radar detection and communication transmission functions, which reduces the hardware, energy consumption, and electromagnetic interference of the mobile platform and also offers higher energy efficiency and spectral efficiency compared to a single system [1–3]. Currently, there are four main application scenarios for integrated radar and communication systems (IRCSs), including unmanned aerial vehicle (UAV) patrol and inspection systems to ensure the safety of the natural environment [4], civil aviation air traffic control systems with automatic real-time tracking [5], military combat systems with real-time target tracking and information sharing [6], and collaborative intelligent transportation systems with environmental awareness and real-time communication [7]. It is worth noting that IRCSs have significant information security issues in different application areas. However, communication information needs to be processed by source coding, channel coding, and information encryption before transmission, which can ensure the accuracy and security of information transmission. It is also very important to

optimize transmitted waveforms and further improve received signal processing for better interoperability and efficiency [8–11].

Orthogonal frequency division multiplexing (OFDM) is a special multicarrier modulation technique that has gained wide attention in the field of digital communications and radar sensing [12–14]. This technology can realize high-speed data transmission by virtue of effectively overcoming intersymbol interference, strong resistance to multipath fading, and high spectrum utilization. Several in-depth studies on integrated waveform design and received signal processing schemes based on OFDM signals can be found in the literature [15–20]. Index modulation, on the other hand, is a reliable modulation technology with high spectrum and energy efficiencies. It transmits information using embedded indexes of building blocks of antennas, subcarriers, spreading codes, and time slots [21,22]. OFDM with index modulation (OFDM-IM) is introduced to take advantage of both technologies. It can flexibly adjust the number and location of activated subcarriers to achieve a favorable compromise between system performance, spectrum utilization, and energy efficiency [23,24]. Because of its flexible design, OFDM-IM has attracted great attention [25,26]. In addition, the multiple-input multiple-output (MIMO) technology is one of the key technologies for future mobile and wireless communication systems, which is characterized by obtaining both reliability and effectiveness gains through the use of spatial resources on the basis of the full utilization of existing spectrum resources. Therefore, MIMO-OFDM technology is also considered as one of the key technologies in 5G or even 6G digital communication [27–29].

By combining the advantages of MIMO technology and OFDM-IM technology, the system proposed in [30] adopts a hybrid analog–digital (HAD) beamforming structure based on MIMO-OFDM-IM, which can be effectively applied to the millimeter wave field. In [31], a feasible solution is proposed by using a Pareto waveform optimization design to approximate the global Pareto optimal compromise between spectrum efficiency and energy efficiency, and it can effectively solve the variational constraint problem in combinatorial optimization models. Based on the signal sparsity characteristics of the MIMO-OFDM-IM system, a low-complexity signal detector based on deep learning (DL) is proposed in [32], which firstly performs the feature information extraction by the acquired signals of the two subnetworks and the DL method, and then the optimized least squares method is used to demodulate the required communication information. It improves the bit error performance and reduces the computational complexity. Paper [33] demonstrated the effect of different signal detection methods on the transmission error bit rate of MIMO-OFDM-IM systems through the derivation of theoretical equations and puts forward its adaptability to visible light communication systems in another reference. In the proposed scheme, the spectral efficiency of the system is greatly improved due to the fact that the OFDM-IM waveforms emitted by each transmitting antenna do not interfere with each other. The method in [34] designs a novel MIMO-OFDM-IM waveform by deactivating a subset of subcarriers. Compared with the conventional MIMO-OFDM waveforms, the subcarrier design of this MIMO-OFDM-IM waveform is more flexible and can achieve a better BER performance, which leads to higher energy efficiency for practical systems. However, the detection of the MIMO-OFDM-IM communication signal becomes a very challenging problem due to the mutual interference between multiple channels and the correlation between different subcarriers of the same subblock [35,36]. In addition, when MIMO-OFDM-IM is applied to radar, it is found that the traditional signal processing method has the problem of dynamic range decline [37,38]. Therefore, under the integrated MIMO-OFDM-IM system, it is urgent to develop more waveform design schemes and corresponding signal processing schemes to improve the system performance.

In this paper, MIMO-OFDM-IM technology is applied to the designed IRCS. After realizing the integrated signal design based on MIMO-OFDM-IM, an improved signal processing scheme is proposed. Firstly, according to the technical characteristics of MIMO-OFDM and IM, an integrated pulse signal design scheme based on MIMO-OFDM-IM is proposed. At the radar receiver, the communication information and phase difference

information of the multipulse echo signal are compensated, and the sparse signal model is obtained by screening the effective data. In addition, a segmented coherent accumulation method based on sparse signal reconstruction is adopted to achieve target parameter estimation within the detection range. At the communication receiver, an improved communication signal detection method based on sequential Monte Carlo is explored. To this end, we summarize our contributions as follows:

(1) The integrated signal design adopts the mode of multiple OFDM symbols in one pulse, which improves the communication transmission rate under the same bandwidth, and IM technology increases the subcarrier frequency spacing, thus having a better intercarrier interference (ICI) resistance capability.

(2) In the integrated MIMO-OFDM-IM systems, an improved method based on information compensation and sparse signal reconstruction is proposed to estimate the range and velocity of radar targets. Compared with the existing methods, it has a better parameter estimation performance.

(3) According to the subcarrier index, we introduce an improved communication signal detection method based on SMC in the proposed system. Compared with the existing methods, the improved method can achieve a lower communication error rate with the same spectral efficiency while ensuring a low computational complexity.

The rest of this paper is organized as follows. In Section 2, we introduce the system model and signal design. In Section 3, the optimized radar and communication signal processing schemes are proposed. In Section 4, we use simulation results to verify the performance of the system. Finally, Section 5 summarizes the main work of this paper.

2. System Model and Signal Design

2.1. System Model

The application scenario we consider is an integrated MIMO-OFDM system with N_t transmitting antennas and N_r receiving antennas, which simultaneously transmit integrated signals to multiple targets and multiple communication users. Each antenna transmits integrated signals in the form of pulses, and each pulse contains multiple OFDM symbols. This transmission mode improves the communication data rate under the same bandwidth. The model of the proposed integrated platform is shown in Figure 1.

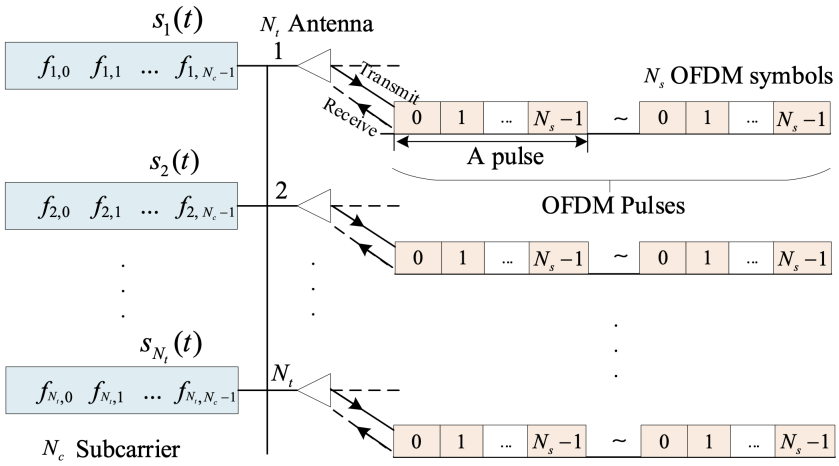


Figure 1. Schematic diagram of the proposed MIMO-OFDM integrated system model.

The transmitted signals of the different antennas in Figure 1 are separated in the frequency domain and only occupy the pre-set continuous frequency spectrum of the whole system's working frequency band. Therefore, the waveforms transmitted by each antenna are orthogonal, which meets the requirements of the MIMO radar for the orthogonality of transmitted waveforms. It is worth mentioning that in order to obtain the subcarrier complex valued weight sequence with the nonoverlapping frequency domain on each

transmitting antenna, we design the subcarrier complex weight sequence by interleaving the structure [39,40].

Next, we apply IM technology to the above integrated MIMO-OFDM system and explore the integrated MIMO-OFDM-IM signal design method. At the transmitter side, the integrated signal design scheme is divided into two stages: the first is bit and subcarrier allocation and the second is the integrated signal design, which is shown in Figure 2.

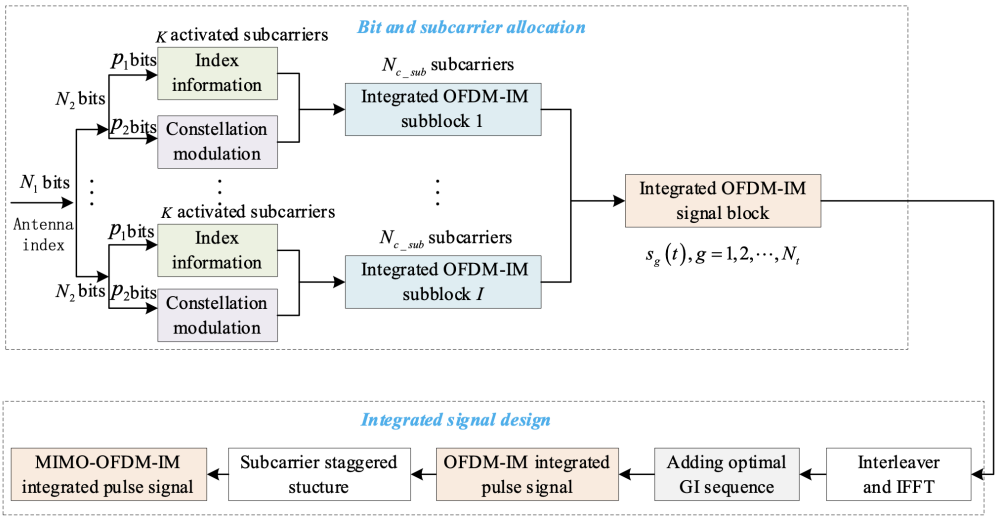


Figure 2. Schematic diagram of MIMO-OFDM-IM integrated signal design in transmitter.

2.2. Bit and Subcarrier Allocation

The main principle of OFDM-IM is to selectively activate some OFDM subcarriers according to the bit stream information and only carry out traditional constellation modulation on the activated subcarriers while the unactivated subcarriers are directly set to zero. After the receiver demodulates the OFDM signal, it can obtain the constellation information on the activated subcarrier, as well as obtain additional index information according to the index position of the activated subcarrier [41]. It is worth noting that the IM equivalently increases the subcarrier frequency spacing, resulting in better ICI resistance.

The allocations of bits and subcarriers are as follows. Assume that the number of bits to be transmitted by the transmitter is N and the bits carried by each antenna are $N_1 = N/N_t$. In addition, to decrease mutual interference between subcarriers, we divide all subcarriers into I subblocks. It is assumed that each antenna has N_c available subcarriers, and then each subblock contains $N_{c_sub} = N_c/I$ subcarriers and $N_2 = N_1/I$ bits.

If K activations are selected from each subblock, there are a total of $C^K_{N_{c_sub}}$ combinations of activated subcarriers, and C is the number of combinations. Therefore, each subblock can transmit $p_1 = \left\lfloor \log_2 C^K_{N_{c_sub}} \right\rfloor$ bits of index information, where $\lfloor \cdot \rfloor$ means rounding down. Meanwhile, the indexes of K activated subcarriers are stored in matrix $\boldsymbol{A}$, and the rest are saved in matrix $\boldsymbol{B}$. In addition, the constellation modulation of M points is performed on the activated subcarriers so that the number of bits of modulation information in each subblock is $p_2 = K \log_2 M$. Suppose that the number of OFDM symbols contained in each pulse signal is N_s, and the modulation information on the kth subcarrier in the mth OFDM symbol is denoted as $d_M(m,k), m = 1,2,\cdots,N_s$; then, the data symbol on the kth subcarrier, mth OFDM symbol, ith subblock, and gth antenna can be formulated as

$$d^i_g(m,k) = \begin{cases} d_M(m,k) & k \in \boldsymbol{A} \\ 0 & k \in \boldsymbol{B} \end{cases} \tag{1}$$

The symbol matrix generated by the ith subblock of gth antennas can be written as

$$\boldsymbol{d}_g^i = \begin{bmatrix} d_g^i(1,1) & d_g^i(1,2) & \cdots & d_g^i(1,N_{c_sub}) \\ d_g^i(2,1) & d_g^i(2,2) & \cdots & d_g^i(2,N_{c_sub}) \\ \vdots & \vdots & \ddots & \vdots \\ d_g^i(N_s,1) & d_g^i(N_s,2) & \cdots & d_g^i(N_s,N_{c_sub}) \end{bmatrix} \tag{2}$$

where $i = 1,2,\cdots,I$ and $g = 1,2,\cdots,N_t$. Each subblock is processed in the same way as described above, and then all the subblocks are concatenated to obtain the OFDM-IM signal block for each antenna, and the obtained bit data matrix on the gth antenna can be represented as

$$\boldsymbol{d}_g = \left[\boldsymbol{d}_g^1, \boldsymbol{d}_g^2, \cdots, \boldsymbol{d}_g^I\right], g = 1,2,\cdots,N_t \tag{3}$$

Assume that the duration of OFDM symbols is T_b. The complex envelope of a pulse signal transmitted on the gth antenna [15] can be written as

$$s_g(t) = \sum_{m=0}^{N_s-1}\sum_{k=0}^{N_c-1} \boldsymbol{d}_g(m,k) \mathrm{e}^{j2\pi k\Delta f(t-mT_b)} \operatorname{rect}\left(\frac{t-mT_b}{T_b}\right) \tag{4}$$

where $\Delta f = 1/T_b$ is the frequency interval of neighboring subcarriers, $\boldsymbol{d}_g(m,k)$ is the element of the mth row and kth column of $\boldsymbol{d}_g$, and rect$(\cdot)$ represents the rectangular window function defined on [0,1].

2.3. Integrated Signal Design

Next, we perform a $I \times N_{c_sub}$ block interleaver and inverse fast Fourier transform (IFFT) on all transmit antennas. In addition, in order to eliminate intersymbol interference (ISI), the guard intervals (GI) sequence should be inserted before all OFDM signal blocks [42]. The traditional way is to directly add a cyclic prefix (CP), but the introduction of a cyclic prefix will produce a high CP sidelobe in radar signal processing, which will affect the target detection performance [43]. Therefore, according to the performance standard of the proposed system, this paper adopts the nonlinear optimization method in [44] to obtain the optimal GI sequences of all OFDM symbols.

Then, after conventional OFDM operations such as serial-to-parallel conversion, the signal is simultaneously transmitted from N_t transmitting antennas via the frequency-selective Rayleigh fading MIMO channel.

According to the above method, all OFDM signals of P pulses are generated, and the total number of activated subcarriers is $K' = K \cdot I \cdot P$. Then, the indexes of the activated subcarriers are arranged in the vector $\boldsymbol{\xi}$ in ascending order, which is expressed as

$$\boldsymbol{\xi} = \begin{bmatrix} \xi_1 & \xi_2 & \cdots & \xi_{K'} \end{bmatrix} \tag{5}$$

where ξ_1, ξ_2, $\cdots$, $\xi_{K'}$ denote the first to K' activated subcarrier indexes, respectively. According to the signal generation flow in Figure 2, the spectral efficiency (in bps/Hz) of the proposed system is given by the following formula:

$$E = \frac{N_t(p_1+p_2)I}{N_c+N_{cp}} = \frac{N_t\left(\left\lfloor \log_2 C_{N_{c_sub}}^K \right\rfloor + K\log_2 M\right)I}{N_c+N_{cp}} \tag{6}$$

It is worth mentioning that the balance among spectrum utilization, transmission reliability, and complexity can be achieved by adjusting relevant parameters in practical applications.

3. Optimized Joint Signal Processing Schemes

In this section, we propose the optimized radar signal processing and communication signal processing schemes. At the radar receiving end, an improved target range and veloc-

ity estimation method based on information compensation and sparse signal reconstruction is introduced. At the communication receiving end, an improved low-complexity detection method based on sequential Monte Carlo is explored. Figure 3 shows the process of the proposed schemes. This figure displays the progressive relationship between different notations, which will be introduced in the next subsection.

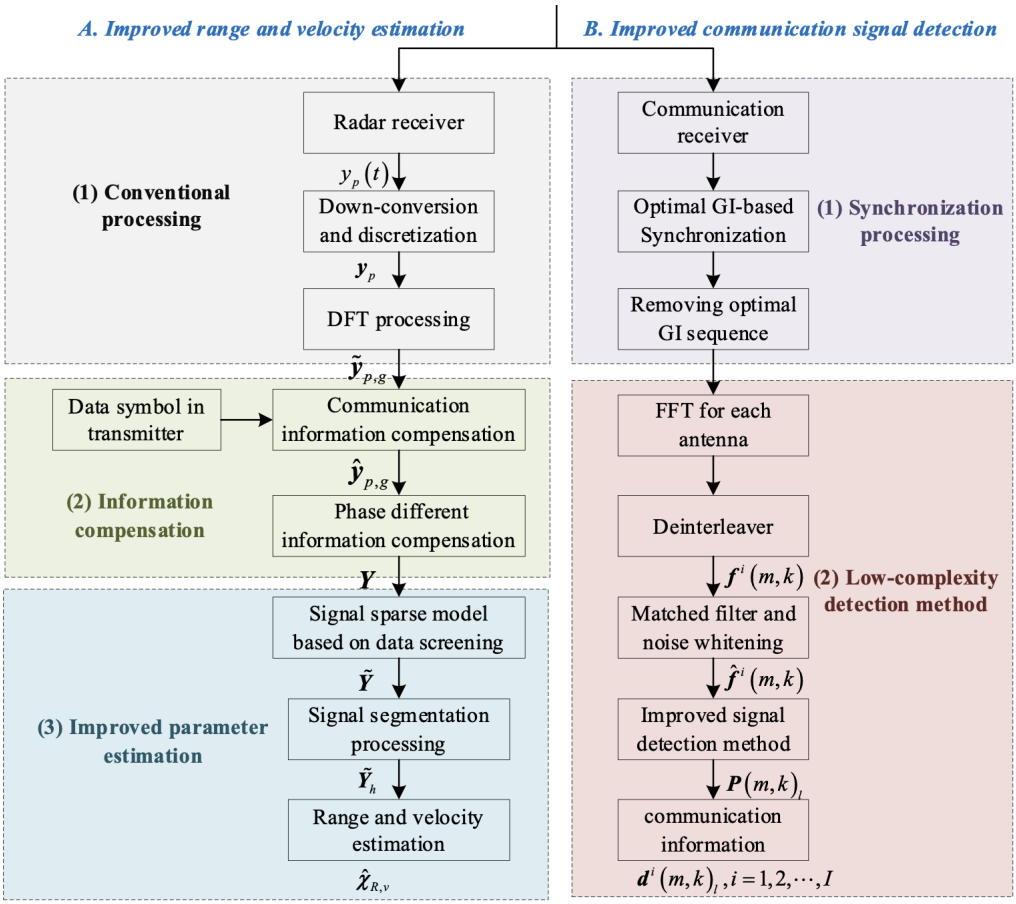


Figure 3. Flow chart of the joint signal processing schemes in the proposed system.

3.1. Sparsity Reconstruction-Based Improved Parameter Estimation

For target echo signals, compared with the MIMO-OFDM system, the subcarriers in the proposed integrated MIMO-OFDM-IM system are sparse, so the variance of the ambiguity function of the integrated signal will increase, which leads to the increase in the sidelobe level obtained by the traditional radar signal processing method. In the theoretical system of compressive sensing, in order to express a signal more accurately, the signal can usually be transformed into a new basis or framework. As long as we know in advance that the signal has sparse expression under this framework, we can reconstruct the transmitted signal. Therefore, we propose a target parameter estimation method based on information compensation and sparse signal reconstruction.

3.1.1. Conventional Processing

The conventional processing of the radar echo signal in the proposed integrated system is shown in Figure 4.

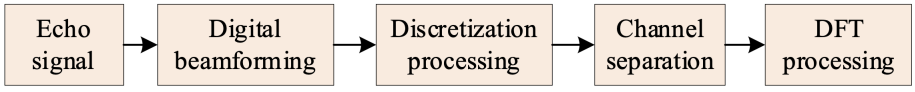


Figure 4. Flowchart of the conventional processing.

Supposing that there are Q detectable targets in the application scenario, the distance between the radar transmitter and the qth target is R_q and the relative velocity of the qth target moving toward the radar is v_q. It can be obtained that the time delay of the qth target is $\tau_q = 2R_q/c$; the Doppler frequency shift is $f_d^q = -2f_c v_q/c$, where f_c is the carrier frequency; and c is the propagation velocity. For simplicity, we suppose that the direction of arrival at the receiving end of the integrated platform is accurately known, and the echo is processed in units of pulses. Then, we can perform digital beamforming; that is, use the aperture of the array antenna to form the receiving beam in the desired direction through digital signal processing so as to form the equivalent single-transmit waveform for the colocated MIMO radar at the receiver [4]. The echo signal of the pth pulse can be formulated as

$$\begin{aligned} y_p(t) &= \boldsymbol{a}_r^H(\theta_r)[y_{p,1}(t), y_{p,2}(t), \cdots, y_{p,N_r}(t)]^{\mathrm{T}} \\ &= N_r \sum_{q=1}^{Q} \beta_q e^{-j2\pi f_c \tau_q} e^{j2\pi f_d^q p T_p} \boldsymbol{a}_t^T(\theta_t) \boldsymbol{s}_p(t-\tau_q) + \omega_p(t) \end{aligned} \tag{7}$$

where $\boldsymbol{a}_r(\theta_r)$ denotes the receive steering vector, β_q is the scattering factor of the qth target, T_p is the pulse repetition period of the transmitted waveform, $\boldsymbol{s}_p(t)$ is the transmitted signal vector of the pth pulse, $\omega_p(t)$ is Gaussian noise, and $\boldsymbol{a}_t(\theta_t)$ indicates the transmit steering vector, and it can be written as

$$\boldsymbol{a}_t(\theta_t) = \left[1, e^{-j2\pi d_t \sin\theta_t/\lambda}, \cdots, e^{-j2\pi(N_t-1)d_t \sin\theta_t/\lambda}\right]^{\mathrm{T}} \tag{8}$$

where d_t is the transmitting antenna spacing and $\lambda = c/f_c$ is the signal wavelength.

Then, the radar-received signal in (7) is sampled at the sampling frequency $f_s = N_c \Delta f$, and the discrete format of the signal in (7) can be denoted as

$$\begin{aligned} \boldsymbol{y}_p =& N_r \sum_{q=1}^{Q} \beta_q e^{j2\pi f_d^q p T_p} \boldsymbol{F}_{N_c}^{-1} \\ & \times \left[\boldsymbol{\psi}_1\left(\tilde{\boldsymbol{s}}_p \odot \boldsymbol{\tau}_q\right), \boldsymbol{\psi}_2\left(\tilde{\boldsymbol{s}}_p \odot \boldsymbol{\tau}_q\right), \cdots, \boldsymbol{\psi}_{N_t}\left(\tilde{\boldsymbol{s}}_p \odot \boldsymbol{\tau}_q\right)\right] \\ & \times \boldsymbol{a}_t(\theta_t) + \boldsymbol{\omega}_p \end{aligned} \tag{9}$$

where $\boldsymbol{\psi}_g$ indicates the diagonal matrix of the gth channel set for realizing the subcarrier interleaving structure, $\odot$ indicates the Hadamard product, $\tilde{\boldsymbol{s}}_p$ indicates the frequency domain weight vector in the pth pulse, and $\boldsymbol{F}_{N_c}^{-1}$ indicates an inverse discrete Fourier transform (IDFT) matrix, which can be written as

$$\boldsymbol{F}_{N_c}^{-1} = \frac{1}{\sqrt{N_c}} \left[e^{j2\pi \frac{(i-1)(j-1)}{N_c}}\right]_{N_c \times N_c}, i, j = 1, 2, \cdots, N_c \tag{10}$$

In addition, $\boldsymbol{\tau}_q$ is the delay vector of the qth target, which is given by

$$\boldsymbol{\tau}_q = \left[e^{-j2\pi f_c \tau_q}, e^{-j2\pi(f_c+\Delta f)\tau_q}, \cdots, e^{-j2\pi(f_c+(N_c-1)\Delta f)\tau_q}\right]^{\mathrm{T}} \tag{11}$$

To minimize the influence of the phase difference information of different channels on the signal processing results, we need to compensate for the received signals of different channels. However, the phase difference information of different channels is different, so it is necessary to separate the channels before compensation. Therefore, according to the structural characteristics of the MIMO-OFDM-IM system, we use the diagonal matrix group in (9) to extract data from different channels through staggered allocation. The received signal of the pth pulse on the gth channel after separation can be represented as

$$\boldsymbol{y}_{p,g} = N_r \sum_{q=1}^{Q} \beta_q e^{j2\pi f_d^q p T_p} e^{-j2\pi(g-1)d_t \sin\theta_t/\lambda} \boldsymbol{F}_{N_c}^{-1} \boldsymbol{\psi}_g \left(\tilde{\boldsymbol{s}}_p \odot \boldsymbol{\tau}_q\right) + \tilde{\boldsymbol{\omega}}_{p,g} \tag{12}$$

Next, we perform N_c-points DFT on the signal in (12) to obtain the following equation

$$\tilde{\mathbf{y}}_{p,g} = N_r \sum_{q=1}^{Q} \beta_q e^{j2\pi f_d^q p T_p} e^{-j2\pi(g-1)d_t \sin\theta_t/\lambda} \boldsymbol{\psi}_g \tilde{\boldsymbol{s}}_p \odot \boldsymbol{\tau}_q + \hat{\boldsymbol{\omega}}_{p,g} \tag{13}$$

where $\hat{\boldsymbol{\omega}}_{p,g} = \tilde{\boldsymbol{\omega}}_{p,g} \boldsymbol{F}_{N_c}$.

3.1.2. Information Compensation

According to the ambiguity function theory of integrated signal in [42], it is known that communication information will affect the echo matching filtering effect, thus reducing the radar detection performance. Based on this, it is necessary to compensate for the signal in (13) in the frequency domain, and the signal compensated by $\tilde{\boldsymbol{s}}_p^{-1}$ can be rewritten as

$$\hat{\mathbf{y}}_{p,g} = N_r \sum_{q=1}^{Q} \beta_q e^{j2\pi f_d^q p T_p} e^{-j2\pi(g-1)d_t \sin\theta_t/\lambda} \boldsymbol{\psi}_g \boldsymbol{\tau}_q + \boldsymbol{W}_{p,g} \tag{14}$$

By stacking all OFDM signals into a matrix, the following formula can be given as

$$\begin{aligned} \boldsymbol{Y}_g =& N_r e^{-j2\pi(g-1)d_t sin\theta_t/\lambda} \boldsymbol{\psi}_g \\ & \times \left[\sum_{q=1}^{Q} \beta_q e^{j2\pi f_d^q T_p} \boldsymbol{\tau}_q, \sum_{q=1}^{Q} \beta_q e^{j2\pi f_d^q 2T_p} \boldsymbol{\tau}_q, \cdots, \sum_{q=1}^{Q} \beta_q e^{j2\pi f_d^q P T_p} \boldsymbol{\tau}_q \right] \\ & + [\boldsymbol{W}_{1,g}, \boldsymbol{W}_{2,g}, \cdots, \boldsymbol{W}_{P,g}] \\ =& N_r e^{-j2\pi(g-1)d_t sin\theta_t/\lambda} \boldsymbol{\psi}_g \sum_{q=1}^{Q} \beta_q \boldsymbol{\tau}_q \otimes \boldsymbol{D}_q^{\mathrm{T}} + \boldsymbol{W}_g \end{aligned} \tag{15}$$

where $\boldsymbol{W}_g = \left[\boldsymbol{W}_{1,g}, \boldsymbol{W}_{2,g}, \cdots, \boldsymbol{W}_{P,g}\right]$, $\otimes$ denotes the Kronecker product of a matrix, and $\boldsymbol{D}_q$ is the Doppler frequency shift vector of the qth target, which can be written as

$$\boldsymbol{D}_q = [e^{j2\pi f_d^q T_p}, e^{j2\pi f_d^q 2T_p}, \cdots, e^{j2\pi f_d^q P T_p}]^{\mathrm{T}} \tag{16}$$

Next, each channel is compensated for phase difference information, and (15) can be rewritten as

$$\boldsymbol{Y} = \sum_{g=1}^{N_t} \boldsymbol{Y}_g e^{j2\pi(g-1)d_t sin\theta_t/\lambda} = N_r \sum_{q=1}^{Q} \beta_q \boldsymbol{\tau}_q \otimes \boldsymbol{D}_q^{\mathrm{T}} + \tilde{\boldsymbol{W}} \tag{17}$$

3.1.3. Improved Parameter Estimation

Generally speaking, the traditional method based on the modulation symbol domain can be used to realize target parameter estimation; that is, we can perform DFT on the signal in (17) along the pulse symbol dimension and perform an IDFT along the subcarrier dimension. Based on this, (17) can be updated to the following formula:

$$\hat{\boldsymbol{Y}} = \boldsymbol{F}_{N_c}^{-1} \boldsymbol{Y} \boldsymbol{F}_P = N_r \sum_{q=1}^{Q} \beta_q \boldsymbol{F}_{N_c}^{-1} \boldsymbol{\tau}_q \otimes \boldsymbol{D}_q^{\mathrm{T}} \boldsymbol{F}_P + \hat{\boldsymbol{W}} \tag{18}$$

where $\boldsymbol{F}_P$ is a discrete Fourier transform (DFT) matrix and its size is $P \times P$. However, due to the use of IM, there may be zero elements in the transmission symbols, which will cause some elements in the matrix $\boldsymbol{Y}$ to converge to infinity. Therefore, it is very difficult to obtain

a good parameter estimation performance by directly adopting the method in (18). We need to extract valid data through data filtering and use new methods to solve it.

According to the relationship between the vectorization of a matrix product and Kronecker product [45], (17) can be transformed into the following formula:

$$\mathrm{vec}(\boldsymbol{Y}) = \mathrm{vec}\left(N_r \sum_{q=1}^{Q} \beta_q \boldsymbol{\tau}_q \otimes \boldsymbol{D}_q^{\mathrm{T}} \right) + \mathrm{vec}(\tilde{\boldsymbol{W}}) \tag{19}$$

where $\mathrm{vec}(\cdot)$ indicates that the matrix is stacked in a vector form by columns. Suppose that $\boldsymbol{R}_q = \boldsymbol{F}_{N_c}^{-1}\boldsymbol{\tau}_q$ and $\boldsymbol{V}_q = \boldsymbol{D}_q^{\mathrm{T}}\boldsymbol{F}_P$. According to the properties of the Kronecker product, (19) can be rewritten as

$$\begin{aligned} \mathrm{vec}(\boldsymbol{Y}) =& \mathrm{vec}\left(N_r \sum_{q=1}^{Q} \beta_q \boldsymbol{F}_{N_c} \boldsymbol{F}_{N_c}^{-1} \boldsymbol{\tau}_q \otimes \boldsymbol{D}_q^{\mathrm{T}} \boldsymbol{F}_P \boldsymbol{F}_P^{-1} \right) + \mathrm{vec}(\tilde{\boldsymbol{W}}) \\ =& \left(\boldsymbol{F}_P^{-\mathrm{H}} \otimes \boldsymbol{F}_{N_c} \right) \mathrm{vec}\left(N_r \sum_{q=1}^{Q} \beta_q \boldsymbol{R}_q \otimes \boldsymbol{V}_q \right) + \mathrm{vec}(\tilde{\boldsymbol{W}}) \end{aligned} \tag{20}$$

where $\boldsymbol{R}_q$ and $\boldsymbol{V}_q$ contain the range and velocity information of the qth target, respectively. According to the index vector $\boldsymbol{\xi}$ of the activated subcarrier in (5), the position of valid data in $\mathrm{vec}(\boldsymbol{Y})$ can be determined. Based on this, we construct a matrix $\boldsymbol{C}$ with the size of $K' \times N_c P$ to filter the data in (20), and its elements can be obtained by the following formula

$$\boldsymbol{C}(i,j) = \begin{cases} 1 & j = \boldsymbol{\xi}(i) \\ 0 & \text{otherwise} \end{cases} \tag{21}$$

According to the characteristics of the matrix and vector, we can filter out invalid data by multiplying (20) by $\boldsymbol{C}$ and extract valid data to realize the sparse reconstruction of the echo signal. After the sparse signal reconstruction of (20), the echo signal model can be reformulated as

$$\tilde{\boldsymbol{Y}} = \tilde{\boldsymbol{C}} \mathrm{vec}\left(N_r \sum_{q=1}^{Q} \beta_q \boldsymbol{R}_q \otimes \boldsymbol{V}_q \right) + \tilde{\boldsymbol{W}}' \tag{22}$$

where

$$\tilde{\boldsymbol{Y}} = \boldsymbol{C} \cdot \mathrm{vec}(\boldsymbol{Y}) \tag{23}$$

$$\tilde{\boldsymbol{C}} = \boldsymbol{C} \cdot (\boldsymbol{F}_P^{-\mathrm{H}} \otimes \boldsymbol{F}_{N_c}) \tag{24}$$

$$\tilde{\boldsymbol{W}}' = \boldsymbol{C} \cdot \mathrm{vec}(\tilde{\boldsymbol{W}}) \tag{25}$$

It can be seen that (22) is a sparse model of received signals corresponding to all targets. In (22), a large matrix dimension will lead to high algorithm complexity. To reduce the complexity of the algorithm, we adopt a segmented coherent accumulation method based on the sparse signal model, and the specific implementation process is as follows:

Assuming that the total number of pulses is P, and it is divided into H equal parts on average, then the number of pulses in each pulse group is $\hat{P} = P/H$. For the hth pulse group data, (22) can be transformed into the following formula:

$$\tilde{\boldsymbol{Y}}_h = \tilde{\boldsymbol{C}}_h \boldsymbol{\chi}_{h,R,v} + \tilde{\boldsymbol{W}}_h' \tag{26}$$

where $\tilde{\boldsymbol{C}}_h = \boldsymbol{C}_h(\boldsymbol{F}_P^{-\mathrm{H}} \otimes \boldsymbol{F}_{N_c})$, $\boldsymbol{C}_h$ is similar to $\boldsymbol{C}$, its size is $K' \times (N_c P/H)$, and $\boldsymbol{\chi}_{h,R,v}$ is a two-dimensional matrix containing range and velocity information, which can be written as

$$\boldsymbol{\chi}_{h,R,v} = N_r \sum_{q=1}^{Q} \beta_q \boldsymbol{R}_q \otimes (\boldsymbol{V}_{q,h}) \tag{27}$$

where

$$\boldsymbol{V}_{q,h} = [e^{j2\pi f_d^q T_p}, e^{j2\pi f_d^q 2T_p}, \cdots, e^{j2\pi f_d^q \hat{P} T_p}]\boldsymbol{F}_{\hat{P}} \tag{28}$$

According to the sparsity of $\boldsymbol{\chi}_{h,R,v}$, (26) can be further equivalently transformed into an optimization problem, which can be described as

$$f^{opt} = \arg\min_{\boldsymbol{\chi}_h} \left(\frac{1}{2} \left\| \tilde{\boldsymbol{Y}}_h - \tilde{\boldsymbol{C}}_h \boldsymbol{\chi}_{h,R,v} \right\|_2^2 + \mu \left\| \boldsymbol{\chi}_{h,R,v} \right\|_1 \right) \tag{29}$$

A large amount of literature points out that there are many methods for solving the unconstrained optimization problem in (29). In this paper, an improved method with low complexity proposed in [46] is used to solve this problem.

After solving the above problem, the matrix $\boldsymbol{\chi}_{h,R,v}$ corresponding to the hth pulse group can be obtained, and then the range dimension information of the pulse group can be obtained by performing an IDFT on this matrix along the pulse group dimension, which can be represented as

$$\boldsymbol{\psi}_{h,R} = \boldsymbol{\chi}_{h,R,v} \boldsymbol{F}_{\hat{P}}^{-1} \tag{30}$$

The H pulse groups are processed according to the above method, and all the results are then recombined. Then, DFT is performed on the reconstructed data, and finally the two-dimensional image information of multiple targets is obtained, which can be denoted as

$$\begin{aligned} \hat{\boldsymbol{\chi}}_{R,v} &= [\boldsymbol{\psi}_{1,R}, \boldsymbol{\psi}_{2,R}, \cdots, \boldsymbol{\psi}_{H,R}]\boldsymbol{F}_P \\ &= \left[\boldsymbol{\chi}_{1,R,v} \boldsymbol{F}_{\hat{P}}^{-1}, \boldsymbol{\chi}_{2,R,v} \boldsymbol{F}_{\hat{P}}^{-1} \cdots, \boldsymbol{\chi}_{H,R,v} \boldsymbol{F}_{\hat{P}}^{-1} \right] \boldsymbol{F}_P \end{aligned} \tag{31}$$

To measure the estimation accuracy of the proposed method based on MIMO-OFDM-IM, we use the Cramér–Rao bound (CRB) as a standard to evaluate all unbiased estimators. Combined with the detailed derivation process in [15], the CRBs of range and velocity under the proposed system are obtained, which can be formulated as

$$\mathrm{CRB}(R) = \frac{I_{vv} c^2}{4(I_{vv} I_{\tau\tau} - I_{v\tau} I_{\tau v})} \tag{32}$$

$$\mathrm{CRB}(v) = \frac{I_{\tau\tau}}{(I_{vv} I_{\tau\tau} - I_{v\tau} I_{\tau v})} \tag{33}$$

where I_{vv}, $I_{\tau\tau}$, $I_{v\tau}$, and $I_{\tau v}$ are the corresponding elements in the Fisher information matrix.

In addition, for the proposed signal design scheme, the range resolution can be expressed as

$$R_{res} = \frac{c}{2B} = \frac{c}{2N_c \Delta f} \tag{34}$$

where c denotes the signal propagation velocity and B denotes the integrated signal bandwidth. In addition, we can effectively determine the maximum detectable range of the proposed system in the environment through the spacing of subcarriers, which can be written as

$$R_{\max} = \frac{c}{2\Delta f} \tag{35}$$

Similarly, the velocity resolution and the maximum detectable velocity of the system are expressed as

$$v_{res} = \frac{c}{2 f_c P T_p} \tag{36}$$

$$v_{\max} = \frac{c}{2 f_c T_p} \tag{37}$$

According to (35), we can realize a larger detection range of the system by reducing the subcarrier spacing. However, (37) shows that the subcarrier spacing should be increased for

a higher detectable velocity. Therefore, it is necessary to choose the appropriate subcarrier spacing according to different requirements in practical applications.

Next, we discuss the computational complexity of the proposed parameter estimation method. First, define one complex multiplication operation as a unit of computational complexity; it is certain that the greater the number of complex multiplications, the higher the computational complexity. According to the processing flow of the above algorithm, the computational complexity of the direct sparse reconstruction of P pulse data is $\mathrm{O}(QKIN_cP^2)$, while the computational complexity of the proposed segmented coherent accumulation method is $H \cdot \mathrm{O}(QKIN_cP^2/H^2) + P^2 \cdot \mathrm{O}(N_c \lg N_c)$.

3.2. Improved Communication Signal Detection

In communication applications, the received signal is the superposition of the transmitted signal polluted by Gaussian noise. The conventional processing of posterior distribution is to search all possible transmitted signal blocks exhaustively, but its complexity is high in the case of large signal blocks. Sequential Monte Carlo (SMC) is an inference method for estimating nonlinear and non-Gaussian state space models, which has been widely used in wireless communication [47,48]. The SMC method approximates the posterior distribution of a state variable by generating high-dimensional Monte Carlo samples dimension by dimension. Specifically, symbol samples are extracted from a defined set in a certain order, and new sequential particles are created by the extracted samples. Then, the importance weight associated with each particle is updated by the probability distribution characteristics. The research shows that the detector based on SMC can achieve a near-maximum likelihood performance while the cost of the receiver is lower. However, the basic SMC can not fully meet the application requirements, so it is necessary to study improved methods suitable for different scenarios. In this section, to reduce the complexity and obtain a better communication performance, we propose an improved SMC signal detection method.

For the communication receiver, we first need to achieve high-precision communication synchronization according to the cross-correlation between all GI sequences and the received communication signal. Then, the interference cancellation method in [49] is adopted to effectively reduce the interference between signals. Meanwhile, the position information of the OFDM signal block carrying modulation symbols is extracted by using the relative position relationship between sequences. All GI sequences will be removed after synchronization is completed. In addition, N_c-point fast Fourier transform (FFT) is adopted at each receiving antenna, and the signal block in the frequency domain is obtained by the $I \times N_{c_sub}$ block deinterleaver. Specifically, for the subcarriers of each OFDM-IM subblock, the received signal vectors of the ith subblock can be stacked as follows:

$$\boldsymbol{f}^i(m,k) = \alpha \left[\boldsymbol{H}^i(m,k)\right]^{\mathrm{T}} \boldsymbol{d}^i(m,k) + \boldsymbol{\omega}^i(m,k) \tag{38}$$

where $\boldsymbol{f}^i(m,k) = \begin{bmatrix} {f_1}^i(m,k) & {f_2}^i(m,k) & \cdots & {f_{N_r}}^i(m,k) \end{bmatrix}^{\mathrm{T}}$ is the received signal vector, α is the balance factor, $\boldsymbol{\omega}^i(m,k)$ is the Gaussian noise vector with zeros mean and unit variance, $\boldsymbol{d}^i(m,k) = \begin{bmatrix} {d_1}^i(m,k) & {d_2}^i(m,k) & \cdots & {d_{N_t}}^i(m,k) \end{bmatrix}^{\mathrm{T}}$ is the modulated transmission signal vector, and $\boldsymbol{H}^i(m,k)$ is the channel frequency responses matrix, which can be written as

$$\boldsymbol{H}^i(m,k) = \begin{bmatrix} h^i_{1,1}(m,k) & h^i_{1,2}(m,k) & \cdots & h^i_{1,N_r}(m,k) \\ h^i_{2,1}(m,k) & h^i_{2,2}(m,k) & \cdots & h^i_{2,N_r}(m,k) \\ \vdots & \vdots & \ddots & \vdots \\ h^i_{N_t,1}(m,k) & h^i_{N_t,N_r}(m,k) & \cdots & h^i_{N_t,N_r}(m,k) \end{bmatrix} \tag{39}$$

To reduce the complexity, we propose an improved communication signal detection method based on SMC. Without changing the noise-whitening characteristics, we need to perform matched filtering and noise whitening on the received signal vector to maximize

the signal-to-noise ratio (SNR). The traditional deterministic SMC algorithm can be used to obtain the noise-whitening matrix [47], which can be written as

$$\boldsymbol{U}^i(m,k) = \left\{ \left[\boldsymbol{H}^i(m,k)\right]^* \left[\boldsymbol{H}^i(m,k)\right]^{\mathrm{T}} \right\}^{\frac{1}{2}} \tag{40}$$

According to the theoretical basis of the continuous interference cancellation method, we perform QR decomposition on the noise whitening matrix obtained in (40), which can be specifically represented as

$$\boldsymbol{U}^i(m,k) = \boldsymbol{Q}^i(m,k)\boldsymbol{R}^i(m,k) \tag{41}$$

where $\boldsymbol{Q}^i(m,k)$ denotes a unitary matrix and $\boldsymbol{R}^i(m,k)$ denotes an upper triangular matrix. After matched filtering, noise whitening, and triangulation of the received signal vector, (38) can be transformed into the following formula:

$$\begin{aligned}
\hat{\boldsymbol{f}}^i(m,k) =& \left[\boldsymbol{Q}^i(m,k)\right]^{\mathrm{H}} \left[\boldsymbol{U}^i(m,k)\right]^{-1} \left[\boldsymbol{H}^i(m,k)\right]^* \boldsymbol{f}^i(m,k) \\
=& \left[\boldsymbol{Q}^i(m,k)\right]^{\mathrm{H}} \left[\left\{ \left[\boldsymbol{H}^i(m,k)\right]^* \left[\boldsymbol{H}^i(m,k)\right]^{\mathrm{T}} \right\}^{\frac{1}{2}} \right]^{-1} \left[\boldsymbol{H}^i(m,k)\right]^* \\
& \times \left\{ \alpha \left[\boldsymbol{H}^i(m,k)\right]^{\mathrm{T}} \boldsymbol{d}^i(m,k) + \boldsymbol{\omega}^i(m,k) \right\} \\
=& \alpha \left[\boldsymbol{Q}^i(m,k)\right]^{\mathrm{H}} \left\{ \left[\boldsymbol{H}^i(m,k)\right]^* \left[\boldsymbol{H}^i(m,k)\right]^{\mathrm{T}} \right\}^{\frac{1}{2}} \boldsymbol{d}^i(m,k) + \hat{\boldsymbol{\omega}}^i(m,k) \\
=& \alpha \boldsymbol{R}^i(m,k)\boldsymbol{d}^i(m,k) + \hat{\boldsymbol{\omega}}^i(m,k)
\end{aligned} \tag{42}$$

Due to the high complexity of directly calculating the posterior probability of each subblock, we adopt a sequential iterative method to numerically approach the true posterior probability infinitely. According to the structure in (42), the symbolic information detection is performed in the order of the antenna index. Since the states of the subcarriers corresponding to each transmitting antenna are independent, the SMC method can iteratively enumerate the symbolic information in the order of the antenna index.

The traversal process of symbol information starts from the first subcarrier, so the number of subcarrier state combinations l_{sub} and the number of samples ε will increase continuously. We set the lower limit value of the number of state combinations as L_{sub} and the upper limit of the number of samples as ε'. The sample extraction process is realized by the important weight of each piece of symbol information.

Combining the results of (42) with the characteristics of maximum likelihood detection, we can obtain the sequence of probability distributions $\boldsymbol{d}^i(m,k)$ conditioned on $\hat{\boldsymbol{f}}^i(m,k)$ as

$$p\left[\hat{\boldsymbol{f}}^i(m,k) | \boldsymbol{d}^i(m,k)\right] = \frac{1}{\pi} e^{-\left|\hat{\boldsymbol{f}}^i(m,k) - \alpha \boldsymbol{R}^i(m,k)\boldsymbol{d}^i(m,k)\right|^2} \tag{43}$$

Suppose that subcarriers in the same subblock are uniformly activated; the prior probability of symbols in any subblock can be expressed as

$$p\left[\boldsymbol{d}_g{}^i(m,k)\right] = \begin{cases} \frac{K}{MN_{c_sub}} & \boldsymbol{d}_g{}^i(m,k) \in d_M(m,k) \\ \frac{N_{c_sub}-K}{N_{c_sub}} & \text{otherwise} \end{cases} \tag{44}$$

Combining the signal model in (42) with the probability distribution function of (43) and (44), the importance weight of each symbol sample for SMC [48] can be represented as

$$\begin{aligned}\boldsymbol{\rho}_g^i(m,k)_j =& \boldsymbol{\rho}_{g-1}^i(m,k)_j p\left[\hat{\boldsymbol{f}}_g^i(m,k)|\kappa_{g-1}^i(m,k)_j\right] \\ =& \boldsymbol{\rho}_{g-1}^i(m,k)_j p\left[\hat{\boldsymbol{f}}_g^i(m,k)|\boldsymbol{d}_g{}^i(m,k), \kappa_{g-1}^i(m,k)_j\right] \\ & \times p\left[\boldsymbol{d}_g{}^i(m,k)\right], j = 1,2,\cdots,\varepsilon\end{aligned} \tag{45}$$

where $\kappa_{g-1}^i(m,k)_j$ is the sample extracted based on subcarriers, and $p\left[\hat{\boldsymbol{f}}_g^i(m,k)|\kappa_{g-1}^i(m,k)_j\right]$ is the prediction distribution of $\boldsymbol{f}_g^i(m,k)$ under the condition of the particles $\kappa_{g-1}^i(m,k)_j$.

According to the comparison results of the importance weight, the L_{sub} state combinations and symbol information corresponding to all subcarriers of each OFDM symbol can be obtained. Then, the posteriori probability corresponding to lth symbol vector can be expressed as

$$\boldsymbol{P}(m,k)_l = p\left[\hat{\boldsymbol{f}}^i(m,k)|\tilde{\boldsymbol{d}}^i(m,k)_l\right] p\left[\tilde{\boldsymbol{d}}^i(m,k)_l\right] \tag{46}$$

where $\tilde{\boldsymbol{d}}^i(m,k)_l$ is the lth symbol vector. We arrange them in descending order by the posteriori probability $\boldsymbol{P}(m,k)_l$. In addition, after N_{c_sub} consecutive detections, the validity of the combination with the largest posterior probability on each subcarrier is also checked sequentially.

To reduce the complexity, we use a combination method to check the legality of all combinations without using a lookup table, which can be written as

$$\gamma = \sum_{k=1}^{K} C_{A_k-1}^k \tag{47}$$

where $\boldsymbol{A}$ denotes the vector storing the indexes of all activated subcarriers. According to (47), this paper regards the state combination of $\gamma < C_{N_{c_sub}}^K$ as legal. Therefore, we can effectively check the legality of all combinations and discard all illegal status combinations. Finally, the legal state combination with the highest posterior probability is selected as the final MIMO-OFDM-IM subblock estimation.

4. Simulation and Numerical Results

In this section, some simulation results are presented to verify the performance of the proposed joint signal processing schemes based on sparse reconstruction in an integrated MIMO-OFDM-IM system. Some parameters required in the simulation are shown in Table 1. In the experiment, we consider an application scenario in which the integrated platform simultaneously sends integrated signals to two targets at a range of 50 m and 100 m, as well as to two communication users, and the velocity of the targets is 20 m/s and 10 m/s, respectively. The integrated platform performs matched filtering and parameter estimation after receiving the echo signal. Meanwhile, the communication users receive and demodulate the communication signals.

Table 1. The parameters of simulation.

Parameters	Value
Bandwidth	20 MHz
Carrier frequency	5 GHz
Duration of pulses	32 μs
Number of OFDM symbols	8
Number of subcarriers	256
Number of subblocks	32
Total number of pulses	32
Lower limit of the number of state combinations	6
Upper limit of the number of samples	10
Modulation mode of communication information	BPSK

4.1. Radar Performance

In this subsection, we verify the radar performance of different radar signal processing methods. To ensure the validity of the comparison results, we set the spectral efficiency of both the MIMO-OFDM system and the MIMO-OFDM-IM system to 4 bps/Hz by adjusting the relevant parameters.

4.1.1. PSLR Performance

First, we pay attention to the peak sidelobe ratio (PSLR) of range and velocity two-dimensional images. The calculation method of the PSLR can be expressed as follows:

$$\mathrm{PSLR} = 10\log_{10}\frac{P_{sl}}{P_{ml}} \tag{48}$$

where P_{sl} denotes the peak level of the highest sidelobe and P_{ml} denotes the peak level of the main lobe.

The PSLR performance of the proposed scheme is shown in Figure 5. In the simulation, $N_t = N_r = 4$, the standard Monte Carlo technique with 10^4 independent trials is used for different SNR levels, and $K = 4$ in Figure 5a. In Figure 5a, the PSLR of the improved method under a different number of pulse groups and the PSLR of the traditional processing method [27] are plotted as a function of the SNR. It can be observed that the PSLR of the traditional FFT method with information compensation gradually decreases with the SNR, but tends to a constant value at a high SNR. This is because this method does not filter the valid data, which leads to the deterioration of the results with the uncertainty of index modulation. However, the PSLR of the proposed method decreases almost linearly with the SNR. Moreover, because a smaller number of pulse groups will result in more pulses in the same pulse group, the PSLR will decrease with the decrease in H. In addition, the PSLR performance of the multichannel is slightly improved compared with that of a single channel. Figure 5b shows the variation in the PSLR of different methods with K under SNR = 10 dB. It can be observed that the PSLR of the traditional FFT method based on information compensation decreases with the increase in K. When $K < 4$, the PSLR drops rapidly with increasing K. On the other hand, when $K > 4$, the PSLR drops very slowly. However, the PSLR of the proposed method is much lower and hardly changes with K under the same SNR, which shows that the uncertainty of index modulation has little influence on the proposed method and the overall performance is better.

Figure 6 shows the variation in the PSLR with the SNR for different methods when K is 3, 5, and 7. It can be found that the PSLR of FFT methods decreases with the increase in the SNR, but when the SNR reaches a certain value, it remains almost unchanged. When all subcarriers in a subblock are activated, the MIMO-OFDM-IM signal reverts to the traditional MIMO-OFDM signal, and the PSLR decreases linearly with an increasing SNR. The PSLR performance of the improved parameter estimation method (IPEM) based on the MIMO-OFDM system in [15] is better compared with the MUSIC algorithm. In contrast, the proposed method has a lower PSLR under the same conditions and decreases with the increase in the SNR. Also, Figure 6 validates that the PSLR performance of the proposed scheme hardly varies with K at different SNRs, which is consistent with the conclusion drawn in Figure 5. It is also noted that, while the IPEM [15] exhibits the same advantage, its performance is consistently about 6dB worse than the proposed method.

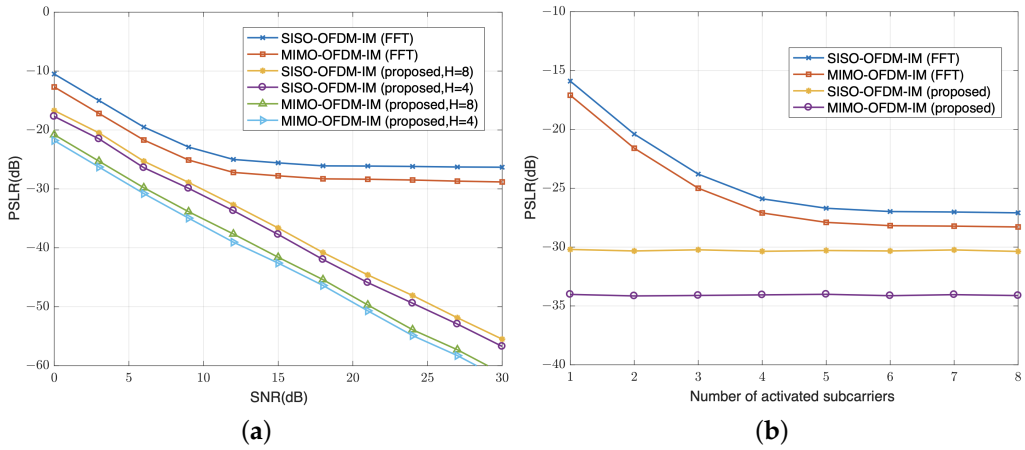


Figure 5. The PSLR performance. (**a**) The variation in PSLR with SNR. (**b**) The variation in PSLR with the number of activated subcarriers (SNR = 10 dB).

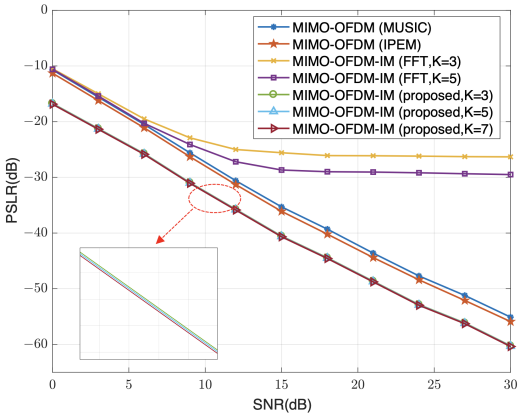
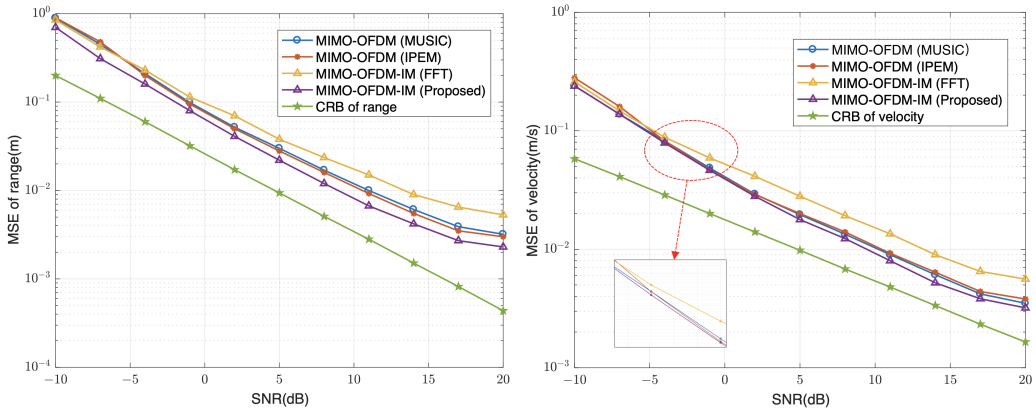


Figure 6. The variation in PSLR with SNR under different number of activated subcarriers.

4.1.2. Range and Velocity Estimation Performance

In order to quantify the target range and velocity estimation performance of the proposed method, Monte Carlo experiments with 10^4 repetitions were carried out under different SNR settings. In the simulation, $K = 4$. The other parameters are as given in Table 1. The four range and velocity estimation methods used for simulation comparisons are as follows: (1) the MUSIC algorithm under the MIMO-OFDM system, (2) the improved parameter estimation method (IPEM) under the MIMO-OFDM system in [15], (3) the FFT algorithm under the MIMO-OFDM-IM system, and (4) the proposed method under the MIMO-OFDM-IM system. Figure 7 shows the variation in the mean-square errors (MSEs) of range and velocity estimation with the SNR under different methods. It can be seen that the MSE of range and velocity estimations both decrease with the increasing SNR. The estimation accuracies of the MUSIC algorithm under the MIMO-OFDM system are basically similar to the published IPEM method in [15], and both are higher than that of the FFT algorithm. In contrast, the proposed method can obtain better estimation accuracy. This is because the proposed method screens the effective data under the designed integrated waveform condition based on MIMO-OFDM-IM. In addition, although the velocity estimation accuracy of the proposed method is better than the methods in the literature and the MUSIC algorithm under the MIMO-OFDM system, its improvement is not as significant as the range estimation improvement, mainly because the proposed method performs FFT on the velocity dimension after dimensionality reduction.

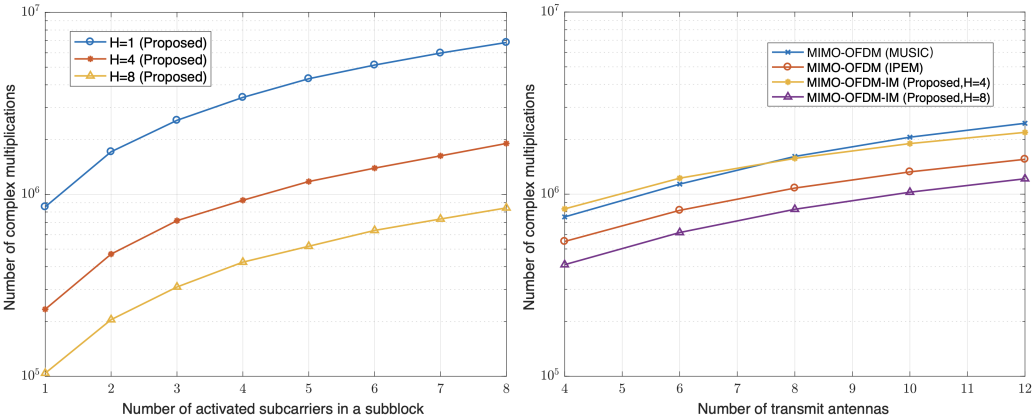


(**a**) (**b**)

Figure 7. The variation in MSEs of range and velocity estimation with SNR under different methods ($N_r = N_t = 4$, $N_{c_sub} = 8$, $K = 4$, $H = 4$). (**a**) Range estimation. (**b**) Velocity estimation.

4.1.3. The Complexity of Parameter Estimation

Figure 8 shows the complexity of the proposed parameter estimation method. In the simulation, 10^4 Monte Carlo experiments were carried out. According to Figure 8a, when $H = 1$, the algorithm does not reduce the dimension, and the number of complex multiplications is large. Having said that, the complexity of the proposed method can be effectively reduced by increasing H, as seen in Figure 8a. In addition, Figure 8b shows that when $H = 4$, the complexity of the proposed system will be slightly higher than that of the MIMO-OFDM system. However, when H is increased to eight, the complexity of the proposed system is greatly reduced, which is lower than the complexity of the improved algorithm in the traditional MIMO-OFDM system. Ultimately, the H to be chosen should be a reasonable compromise between the algorithm complexity and parameter estimation performance.



(**a**) (**b**)

Figure 8. Complexity comparison. (**a**) The variation in number of complex multiplications with the number of activated subcarriers. (**b**) The variation in number of complex multiplications with the number of transmitting antennas.

4.2. Communication Performance

4.2.1. BER Performance

In this subsection, the bit error rate (BER) performance of the proposed signal detection method for the integrated MIMO-OFDM-IM system is evaluated via Monte Carlo

simulations with 10^4 trials. In this simulation, the communication symbol is modulated by BPSK modulation. Similar to the previous section, the spectral efficiency is uniformly set to 4 bps/Hz. Five detection methods are used for comparative analysis, including the maximum likelihood (ML) detection method, minimum mean square error (MMSE) detection method, improved MMSE detection method [50], subblock-wise detection method [51], and the proposed method. In Figure 9, the BER of different methods for different SNR levels is depicted with $N_r = N_t = 4$. According to the result of Figure 9a, it can be observed that the performance loss of the MMSE detection method is substantial, whilst the performance of the improved MMSE detection method has improved, albeit not significantly. In contrast, the performance of the subblock-wise detection method has greatly improved. Finally, the proposed detection method achieves a better BER performance and has only a small performance loss compared with the ML detection method. A further comparison shows that, with an increasing K (Figure 9b), the BER performance of all detection methods decreases slightly, mainly because the modulation symbols to be detected will increase with the increase in K. In this case, the performance of the proposed method is still slightly better than the subblock-wise detection method, and both methods are still very close to the ML detection method.

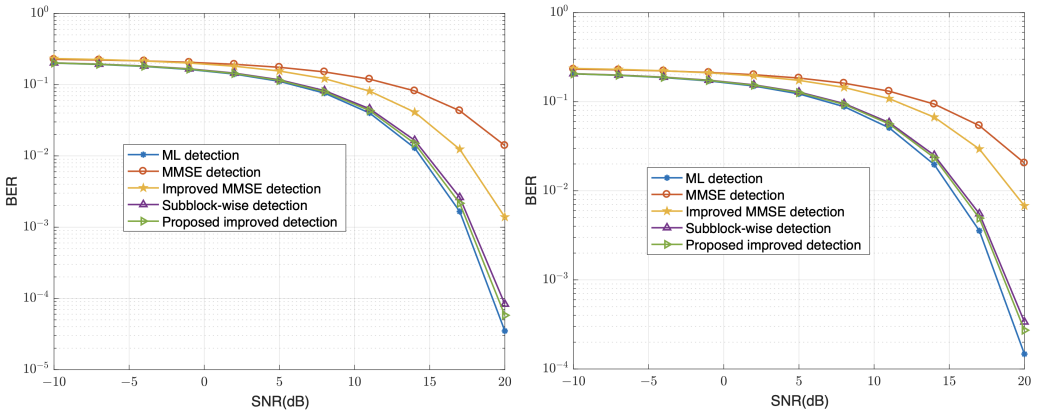


Figure 9. The BER performance of different information detection methods under the proposed integrated MIMO-OFDM-IM system ($N_r = N_t = 4$). (**a**) $N_{c_sub} = 8$, $K = 3$; (**b**) $N_{c_sub} = 8$, $K = 6$.

Figure 10 shows the BER performances of different detection methods for different SNR levels with $N_r = N_t = 8$. As seen from Figure 10, the BER performance of the ML detection method, subblock-wise detection method, and the proposed detection method are obviously superior to other detection methods. Comparing Figure 10 with Figure 9, it can be observed that the BER performances of all information detection methods have obviously improved with the increase in the number of transmitting and receiving antennas. In particular, the performance of the subblock-wise detection method is closer to that of the proposed information detection method. However, the algorithm complexity of the subblock-wise detection method is significantly higher than that of the proposed method, which will be shown in the statistical results of the algorithm complexity later. It is worth mentioning that the ML detection method has a better BER performance than other methods, but its algorithm complexity is very high. Comparing Figure 10a and Figure 10b, it can be observed that all information detection methods are sensitive to K.

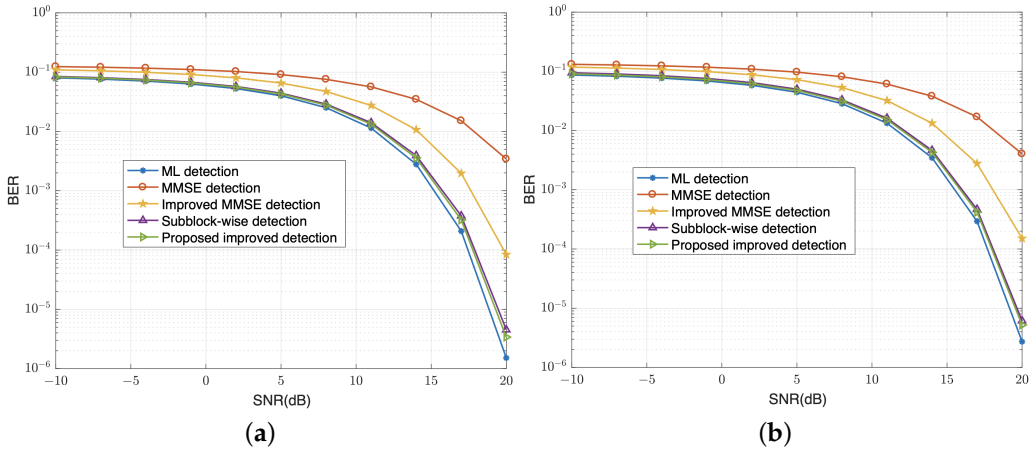


Figure 10. The BER performance of different information detection methods under the proposed integrated MIMO-OFDM-IM system ($N_r = N_t = 8$). (**a**) $N_{c_sub} = 8$, $K = 3$; (**b**) $N_{c_sub} = 8$, $K = 6$.

4.2.2. The Complexity of Communication Detection Methods

In the following analysis, the number of complex multiplications is used as an evaluation indicator of algorithm complexity. The number of complex multiplications of different detection methods under the same parameter conditions is shown in Table 2. Obviously, the complexity of the ML detection method is very high, and with the increasing N_t, its complexity increases exponentially. An MMSE-based detection method can effectively reduce the computational complexity, but its BER performance is not great, as has been observed earlier. In contrast, the improved detection method based on SMC can effectively improve the information detection performance while ensuring the algorithm complexity. Especially, with the increase in N_t, the complexity of the proposed method is lower than that of the subblock-wise detection method. Generally speaking, the signal detection method under the integrated MIMO-OFDM-IM system can ensure stable synchronization and a relatively good communication information detection performance.

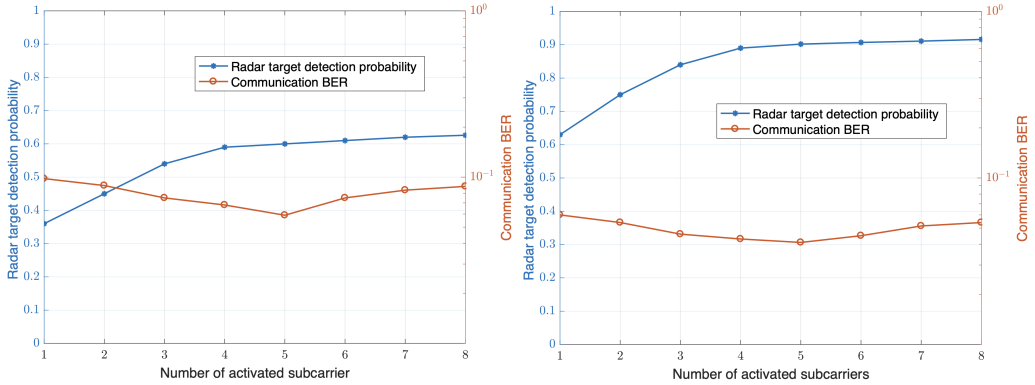
Table 2. Algorithm complexity comparison of different detection methods.

Parameters	**Number of Complex Multiplications**		
	$N_t = 4$	$N_t = 8$	$N_t = 12$
ML detection	3.26×10^6	–	–
MMSE detection	6.62×10^2	5.28×10^3	9.35×10^3
Improved MMSE detection	2.07×10^3	9.23×10^3	2.84×10^4
Subcarrier-wise detection	2.23×10^3	8.51×10^3	1.5×10^4
Proposed improved detection	2.27×10^3	6.04×10^3	9.61×10^3

4.3. Trade-Off Performance

In the integrated MIMO-OFDM-IM system, to evaluate the influence of different activated subcarrier combinations on system performance, we constructed a trade-off curve between radar and communication through simulations employing different activated subcarrier combinations, and the trade-off parameters include radar target detection probability and communication BER. In the simulations, we carried out 10^4 Monte Carlo experiments, and in each experiment, the target was detected in the radar monitoring range. Figure 11 shows the variation in the radar–communication trade-off curve with the number of activated subcarriers under different SNRs. It can be found that the radar target detection probability increases monotonically with K and becomes stable when the number equals or is more than five. On the other hand, when $K = 5$, the communication BER performance is the best. Therefore, the appropriate activated subcarrier combinations can

be selected according to different requirements of the actual environment, while a general rule-of-thumb approach would be using five activated subcarriers since it gives the best communication performance and relatively high target detection probability.



(**a**) (**b**)

Figure 11. The variation in radar–communication trade-off curve with the number of activated subcarriers under different SNRs ($N_r = N_t = 4$). (**a**) SNR = 6 dB; (**b**) SNR = 12 dB.

5. Conclusions

In this paper, a sparse reconstruction-based joint signal processing scheme for integrated MIMO-OFDM-IM systems is proposed, which can achieve a higher target range and velocity estimation accuracy and lower communication BER under the same spectral efficiency. According to the combination of MIMO-OFDM and IM technology, the waveform design based on the MIMO-OFDM-IM integrated system is realized. For radar, after conventional processing and information compensation, a segmented coherent accumulation method based on sparse signal reconstruction is used to realize parameter estimation. The numerical results show that the proposed method can achieve a better PSLR performance and higher accuracy of range and velocity estimation. For communication, we use the subcarriers corresponding to the OFDM symbols of each subblock as a benchmark; the information samples are detected iteratively through an antenna index; and the information symbols are obtained through a series of processes such as weight updating, screening, and sorting. The simulation experiment proved that the proposed scheme has a high information transmission efficiency and good communication information detection performance. In the future, sn MIMO-OFDM waveform design based on adaptive, robust, and PAPR reduction will be our research focus. The optimized waveform design can further solve the problems of radar–communication performance trade-off and algorithm practicability.

Author Contributions: Y.W. and Y.C. (Yunhe Cao) developed the theory and signal model. Y.W. and Y.C. (Yunhe Cao) performed and analyzed the numerical simulations. Y.W., T.-S.Y., Y.C. (Yuanhao Cheng) and Y.Z. wrote and edited the paper. All authors have read and agreed to the published version of the manuscript.

Funding: This work was funded by the National Nature Science Foundation of China under grant 61771367.

Data Availability Statement: The data presented in this study are available upon request from the corresponding author. The data are not publicly available due to restrictions, e.g., privacy or ethics.

Conflicts of Interest: The authors declare no conflicts of interest.

Abbreviations

The following abbreviations are used in this manuscript:

OFDM	orthogonal frequency division multiplexing
IM	index modulation
IRCS	integrated radar and communication systems
UAV	unmanned aerial vehicle
MIMO	multiple-input multiple-output
HAD	hybrid analog–digital
DL	deep learning
ICI	intercarrier interference
IFFT	inverse fast Fourier transform
CP	cyclic prefix
GI	guard interval
ISI	intersymbol interference
DFT	discrete Fourier transform
CRB	Cramér–Rao bound
SMC	sequential Monte Carlo
SNR	signal-to-noise ratio
PSLR	peak sidelobe ratio
MSE	mean-square error
BER	bit error rate
ML	maximum likelihood
MMSE	minimum mean square error

References

1. Kumari, P.; Choi, J.; González-Prelcic, N.; Heath, R.W. IEEE 802.11ad-Based Radar: An Approach to Joint Vehicular Communication-Radar System. *IEEE Trans. Veh. Technol.* **2018**, *67*, 3012–3027. [CrossRef]
2. Grossi, E.; Lops, M.; Venturino, L. Joint Design of Surveillance Radar and MIMO Communication in Cluttered Environments. *IEEE Trans. Signal Process.* **2020**, *68*, 1544–1557. [CrossRef]
3. Gu, M.-X.; Lee, M.-C.; Liu, Y.-S.; Lee, T.-S. Design and Analysis of Frequency Hopping-Aided FMCW-Based Integrated Radar and Communication Systems. *IEEE Trans. Commun.* **2022**, *70*, 8416–8432. [CrossRef]
4. Zhang, J.; Liu, F.; Masouros, C.; Heath, R.; Feng, Z.; Zheng, L.; Petropulu, A. An overview of signal processing techniques for joint communication and radar sensing. *IEEE J. Sel. Topics Signal Process.* **2021**, *15*, 1295–1315. [CrossRef]
5. Wang, J.; Liang, X.-D.; Chen, L.-Y.; Li, Y.-L. Waveform Designs for Joint Wireless Communication and Radar Sensing: Pitfalls and Opportunities. *IEEE Internet Things J.* **2023**, *10*, 15252–15265. [CrossRef]
6. Xiao, Z.; Zeng, Y. Waveform design and performance analysis for full-duplex integrated sensing and communication. *IEEE J. Sel. Areas Commun.* **2022**, *40*, 1823–1837. [CrossRef]
7. Liu, F.; Masouros, C.; Petropulu, A.P.; Griffiths, H.; Hanzo, L. Joint Radar and Communication Design: Applications, State-of-the-Art, and the Road Ahead. *IEEE Trans. Commun.* **2020**, *68*, 3834–3862. [CrossRef]
8. Wang, Y.; Cao, Y.; Yeo, T.-S.; Cheng, Y.; Fu, J. Robust Multiplexing Waveform Design for Integrated OFDM Radar and Communication via Complex Weight Optimization. *Remote Sens.* **2023**, *15*, 4438. [CrossRef]
9. Liu, F.; Zhou, L.; Masouros, C.; Li, A.; Luo, W.; Petropulu, A. Toward Dual-functional Radar-Communication Systems: Optimal Waveform Design. *IEEE Trans. Signal Process.* **2018**, *66*, 4264–4279. [CrossRef]
10. Yu, X.; Yao, X.; Yang, J.; Zhang, L.; Kong, L.; Cui, G. Integrated Waveform Design for MIMO Radar and Communication via Spatio-Spectral Modulation. *IEEE Trans. Signal Process.* **2022**, *70*, 2293–2305. [CrossRef]
11. Zheng, L.; Lops, M.; Eldar, Y. C.; Wang, X. Radar and Communication Coexistence: An Overview: A Review of Recent Methods. *IEEE Signal Process. Mag.* **2019**, *36*, 85–99. [CrossRef]
12. Hwang, S.; Seo, J.; Park, J.; Kim, H.; Jeong, B.J. Compressive Sensing-Based Radar Imaging and Subcarrier Allocation for Joint MIMO OFDM Radar and Communication System. *Sensors* **2021**, *21*, 2382. [CrossRef] [PubMed]
13. Rong, J.; Liu, F.; Miao, Y. High-Efficiency Optimization Algorithm of PMEPR for OFDM Integrated Radar and Communication Waveform Based on Conjugate Gradient. *Remote Sens.* **2022**, *14*, 1715. [CrossRef]
14. Yamamoto, H.; Nakamura, A.; Itami, M. A study on LDM-BST-OFDM transmission for the next-generation terrestrial broadcasting. *IEEE Trans. Broadcast.* **2020**, *66*, 205–215. [CrossRef]
15. Liu, Y.; Liao, G.; Chen, Y.; Xu, J.; Yin, Y. Super-resolution range and velocity estimations with OFDM integrated radar and communications waveform. *IEEE Trans. Veh. Technol.* **2020**, *69*, 11659–11672. [CrossRef]
16. Liu, Y.; Liao, G.; Xu, J.; Yang, Z.; Huang, L.; Zhang, Y. Transmit power adaptation for orthogonal frequency division multiplexing integrated radar and communication systems. *J. Appl. Remote Sens.* **2017**, *11*, 035017. [CrossRef]

17. Shi, C.; Wang, F.; Salous, S.; Zhou, J. Joint subcarrier assignment and power allocation strategy for integrated radar and communications system based on power minimization. *IEEE Sens. J.* **2019**, *19*, 11167–11179. [CrossRef]
18. Temiz, M.; Alsusa, E.; Baidas, M.W. A dual-functional massive MIMO OFDM communication and radar transmitter architecture. *IEEE Trans. Veh. Technol.* **2020**, *69*, 14974–14988. [CrossRef]
19. Keskin, M.F.; Koivunen, V.; Wymeersch, H. Limited feedforward waveform design for OFDM dual-functional radar-communications. *IEEE Trans. Signal Process.* **2021**, *69*, 2955–2970. [CrossRef]
20. Ahmed, A.; Zhang, Y.D.; Hassanien, A. Joint Radar-Communications Exploiting Optimized OFDM Waveforms. *Remote Sens.* **2021**, *13*, 4376. [CrossRef]
21. Saad, M.; Palicot, J.; Bader, F.; Ghouwayel, A.C.A.; Hijazi, H. A Novel Index Modulation Dimension Based on Filter Domain: Filter Shapes Index Modulation. *IEEE Trans. Commun.* **2021**, *69*, 1445–1461. [CrossRef]
22. Yu, P.; Huang, F. Spatial Index Modulation with the Combination of Both Antenna Indexes and Two Constellations. *IEEE Access* **2022**, *10*, 133778–133788. [CrossRef]
23. Choi, J. Coded OFDM-IM With Transmit Diversity. *IEEE Trans. Commun.* **2017**, *65*, 3164–3171. [CrossRef]
24. Zhu, Y.; Wang, B.; Li, J.; Zhang, Y.; Xie, F. Y-Shaped Net-Based Signal Detection for OFDM-IM Systems. *IEEE Commun. Lett.* **2022**, *26*, 2661–2664. [CrossRef]
25. Li, J.; Dang, S.; Huang, Y.; Chen, P.; Qi, X.;Wen, M.; Arslan, H. Composite Multiple-Mode Orthogonal Frequency Division Multiplexing with Index Modulation. *IEEE Trans. Wireless Commun.* **2023**, *22*, 3748–3761. [CrossRef]
26. Sui, Z.; Yan, S.; Zhang, H.; Yang, L.-L.; Hanzo, L. Approximate Message Passing Algorithms for Low Complexity OFDM-IM Detection. *IEEE Trans. Veh. Technol.* **2021**, *70*, 9607–9612. [CrossRef]
27. Xu, Z.; Petropulu, A. A Bandwidth Efficient Dual-Function Radar Communication System Based on a MIMO Radar Using OFDM Waveforms. *IEEE Trans. Signal Process.* **2023**, *71*, 401–416. [CrossRef]
28. Xu, J.; Zhou, Z.; Li, L.; Zheng, L.; Liu, L. RC-Struct: A Structure-Based Neural Network Approach for MIMO-OFDM Detection. *IEEE Trans. Wirel. Commun.* **2022**, *21*, 7181–7193. [CrossRef]
29. Qian, J.; Lops, M.; Zheng, L.; Wang, X.; He, Z. Joint System Design for Coexistence of MIMO Radar and MIMO Communication. *IEEE Trans. Signal Process.* **2018**, *66*, 3504–3519. [CrossRef]
30. Basar, E. Multiple-input multiple-output OFDM with index modulation. *IEEE Signal Process. Lett.* **2015**, *22*, 2259–2263. [CrossRef]
31. Yang, Y.; Dang, S.; Wen, M.; Guizani, M. Millimeter Wave MIMO-OFDM with Index Modulation: A Pareto Paradigm on Spectral-Energy Efficiency Trade-Off. *IEEE Trans. Wirel. Commun.* **2021**, *20*, 6371–6386. [CrossRef]
32. Zhao, T.; Li, F. Variational-autoencoder signal detection for MIMO-OFDM-IM. *Digit. Signal Process.* **2021**, *118*, 103230. [CrossRef]
33. Basar, E. On multiple-input multiple-output OFDM with index modulation for next generation wireless networks. *IEEE Trans. Signal Process.* **2016**, *64*, 3868–3878. [CrossRef]
34. Wang, L. Generalized Quadrature Space-Frequency Index Modulation for MIMO-OFDM Systems. *IEEE Trans. Commun.* **2021**, *69*, 6375–6389. [CrossRef]
35. Hodge, J.A.; Mishra, K.V.; Zaghloul, A.I. Intelligent Time-Varying Metasurface Transceiver for Index Modulation in 6G Wireless Networks. *IEEE Antennas Wirel. Propag. Lett.* **2020**, *19*, 1891–1895. [CrossRef]
36. Chen, R.; Zheng, J. Index-Modulated MIMO-OFDM: Joint Space-Frequency Signal Design and Linear Precoding in Rapidly Time-Varying Channels. *IEEE Trans. Wirel. Commun.* **2018**, *17*, 7067–7079. [CrossRef]
37. Noh, H.; Lee, H.; Yang, H.J. IICI-Robust Transceiver Design for Integration of MIMO-OFDM Radar and MU-MIMO Communication. *IEEE Trans. Veh. Technol.* **2023**, *72*, 821–838. [CrossRef]
38. Schindler, D.; Schweizer, B.; Knill, C.; Hasch, J.; Waldschmidt, C. Synthetization of Virtual Transmit Antennas for MIMO OFDM Radar by Space-Time Coding. *IEEE Trans. Aerosp. Electron. Syst.* **2021**, *57*, 1964–1971. [CrossRef]
39. Hakobyan, G.; Ulrich, M.; Yang, B. OFDM-MIMO Radar With Optimized Nonequidistant Subcarrier Interleaving. *IEEE Trans. Aerosp. Electron. Syst.* **2020**, *56*, 572–584. [CrossRef]
40. Multerer, T.; Prechtel, U.; Vossiek, M.; Ziegler, V. Systematic Phase Correction for Direction-of-Arrival Estimation in Spectrally Interleaved OFDM MIMO Radar. *IEEE Trans. Microw. Theory Technol.* **2019**, *67*, 4570–4577. [CrossRef]
41. Zhang, S.-Y.; Shahrrava, B. A SLM Scheme for PAPR Reduction in Polar Coded OFDM-IM Systems Without Using Side Information. *IEEE Trans. Broadcast.* **2021**, *67*, 463–472. [CrossRef]
42. Deng, S. Reduced-Guard-Interval OFDM Using Digital Sub-Band-Demultiplexing. *IEEE Photon. Technol. Lett.* **2013**, *25*, 2174–2177. [CrossRef]
43. Liu, Y.; Yi, J.; Wan, X.; Zhang, X.; Ke, H. Evaluation of Clutter Suppression in CP-OFDM-Based Passive Radar. *IEEE Sens. J.* **2019**, *19*, 5572–5586. [CrossRef]
44. Wang, Y.; Cao, Y.; Yeo, T.-S.; Han, J.; Peng, Z. Joint Sequence Optimization-Based OFDM Waveform Design for Integrated Radar and Communication Systems. *IEEE Trans. Veh. Technol.* **2022**, *71*, 12734–12748. [CrossRef]
45. Roth, I.; Kliesch, M.; Flinth, A.; Wunder, G.; Eisert, J. Reliable Recovery of Hierarchically Sparse Signals for Gaussian and Kronecker Product Measurements. *IEEE Trans. Signal Process.* **2020**, *68*, 4002–4016. [CrossRef]
46. Chen, Y.; Liu, Y.; Chen, J.; Ma, J. A Novel Identification Method for a Class of Closed-Loop Systems Based on Basis Pursuit De-Noising. *IEEE Access* **2020**, *8*, 99648–99654. [CrossRef]
47. Vesa, J.; Rasilo, P. Permeability Estimations of SMC Material Particles. *IEEE Trans. Magn.* **2020**, *56*, 2000807. [CrossRef]

48. Wang, Y.; Xia, Y.; Shen, H.; Zhou, P. SMC Design for Robust Stabilization of Nonlinear Markovian Jump Singular Systems. *IEEE Trans. Autom. Control* **2018**, *63*, 219–224. [CrossRef]
49. Yih, C. Iterative interference cancellation for OFDM signals with blanking nonlinearity in impulsive noise channels. *IEEE Signal Process. Lett.* **2012**, *19*, 147–150. [CrossRef]
50. Fang, L.; Xu, L.; Huang, D.D. Low Complexity Iterative MMSE-PIC Detection for Medium-Size Massive MIMO. *IEEE Wirel. Commun. Lett.* **2016**, *5*, 108–111. [CrossRef]
51. Zheng, B.; Wen, M.; Basar, E.; Chen, F. Multiple-Input Multiple-Output OFDM With Index Modulation: Low-Complexity Detector Design. *IEEE Trans. Signal Process.* **2017**, *65*, 2758–2772. [CrossRef]

Disclaimer/Publisher's Note: The statements, opinions and data contained in all publications are solely those of the individual author(s) and contributor(s) and not of MDPI and/or the editor(s). MDPI and/or the editor(s) disclaim responsibility for any injury to people or property resulting from any ideas, methods, instructions or products referred to in the content.